Modes of Adhesion of Spherocylindrical Nanoparticles to Tensionless Lipid Bilayers

Abash Sharma, Yu Zhu, Eric J. Spangler, and Mohamed Laradji*
Department of Physics and Materials Science, The University of Memphis, Memphis, TN 38152, USA

The adhesion modes and endocytosis pathway of spherocylindrical nanoparticles (NPs) are investigated numerically using molecular dynamics simulations of a coarse-grained implicit-solvent model. The investigations is performed systematically with respect to the adhesion energy density ξ , NP's diameter D, and NP's aspect ratio α . At weak ξ , the NP adheres to the membrane through a parallel mode, i.e. such that its principal axis is parallel to the membrane. However, for relatively large ξ , the NP adheres through a perpendicular mode, i.e. the NP is invaginated such as its principal axis is nearly perpendicular to the membrane. The value of ξ at the transition from the parallel to the perpendicular mode decreases with increasing the D or α , in agreement with theoretical arguments based on the Helfrich Hamiltonian. As ξ is further increased, the NP undergoes endocytosis, with the value of ξ at the endocytosis threshold that is independent of the aspect ratio but decreases with increasing D. The kinetics of endocytosis depends strongly on ξ and D. While for low values of D, the NP first rotates to a parallel orientation then to a perpendicular orientation. At high values of ξ or D, the NP is endocytosed while in the parallel orientation.

I. INTRODUCTION

Recent advances in nanoscience and nanotechnology has accelerated the fabrication of nanomaterials with different geometries, dimensions and surface properties [1]. Engineered nanomaterials can be designed for use in different applications including chemical sensing [2, 3], electronics [4], data storage [5], food industry [6], and cosmetics [7]. A particularly astonishing progress has been made in the development of nanomaterials for various biological and medical applications. These include gene therapy [8], cancer drug delivery [9], cancer diagnostics [10], biosensing [11], and the probe of intracellular structure [12]. With the ever-increasing range of applications of nanomaterials, there is also a growing need to investigate their potential toxicity and ways to minimize it [13–15]. The development of effective and safe nanomaterials requires an understanding of how nanoparticles (NPs) interact with biomembranes, which act as the entry point of living cells.

Many NPs properties depend highly on their morphology. For example, gold NPs with tailored optical properties can be synthesized by tuning their morphology, making them uniquely promising for a range of biomedical applications [16]. Several studies have shown that NPs dimensions and geometry play a major role on their adhesion to lipid membranes and their internalization [17–21]. Gratton et al.'s study, in particular, showed that internalization of cylindrical NPs with a given aspect ratio is enhanced with increasing the NPs diameter [18]. The uptake of NPs by living cells is complicated by the presence of several active processes facilitating their internalization. Furthermore, the actomyosin cytoskeleton may hinder the adhesion mode in which the NPs pro-

trude to the inner side of the cell. The understanding of the effect of NPs morphology on their adhesion on cells and their subsequent internalization would greatly benefit from studies of the adhesion of NPs on simple lipid membranes. Unfortunately, systematic experimental investigations of the adhesion and internalization of non-spherical NPs by simple model lipid membranes have thus far been largely lacking. This makes computer simulations a useful alternative tool to understand the adhesion and internalization of non-spherical NPs by lipid membranes.

The onset and modes of adhesion of NPs to lipid membranes can be estimated from the balance between the adhesive energy and the membrane elasticity energy. In the simplest case of a spherical NP with diameter D, its adhesion energy is $E_{adh} = -\pi \nu D^2 \xi$, where $\xi(>0)$ is the adhesion energy density and ν is the fraction of the NP's surface in contact with the membrane. In the case of a tensionless planar membrane, its excess elastic energy, resulting from its curvature deformation, due to the adhesion of the NP, is $E_{curv} = 8\pi\nu\kappa$, where κ is the membrane bending modulus. The minimization of the total energy leads to an adhesion threshold $\xi^* = 8\kappa/D^2$, below which the NP is unbound and above which, the NP is fully wrapped by the membrane ($\nu = 1$) [22, 23]. This argument assumes that the NP and the membrane interact with each other only when they are in contact and that the curvature energy of the non-contact portion of the membrane is zero. This argument was shown to not be correct if the NPs diameter is comparable to, or few times, the thickness of the lipid membrane or if the finite range of the NP-membrane interaction is accounted for [24–26].

The arguments above can be extended to the case of a cylindrical NP, with diameter D and very high aspect ratio, such that its two ends can be ignored. In this case, one finds that the NP adheres to the membrane for $\xi > \xi^* = 2\kappa/D^2$. The decrease in the adhesion threshold of a cylindrical NP is due to its reduced mean curvature

^{*}mlaradji@memphis.edu

compared to that of a spherical NP with same diameter. The adhesion of spherocylindrical NPs on lipid membranes and their endocytosis was investigated through coarse-grained molecular dynamics (MD) simulations by Vácha et al. [19] and Huang et al. [20]. Both studies focussed on the kinetics of spontaneous endocytosis of NPs with ligands that bind to a fraction of lipids (receptors), and on the case where the adhesion energy density is relatively high. Huang et al. found that an NP, with aspect ratio higher than about 2, first adheres through its cylindrical side to the membrane [20]. When the NP is about half-wrapped, it rotates to a perpendicular orientation [20]. Finally the NP is endocytosed while nearly perpendicular to membrane plane [20]. On the other hand, Vácha et al. found, using a more microscopic membrane model, that while the NP adheres through its cylindrical side to the membrane, they are endocytosed while they remain nearly parallel to the membrane's plane [19].

The modes of adhesion of cylindrical NPs, with finite aspect ratio and blunt circular ends, was investigated by Dasgupta et al. [21] using a Monte Carlo energy minimization method of dynamically triangulated planar membranes. For low values of ξ , the NP adheres shallowly to the membrane through one of its blunt surfaces for high values of the curvature, c_{edge} , of the circular edges between the NP's cylindrical side and blunt surfaces or for low values of the NP's aspect ratio, α . However, for low values of c_{edge} or high values of α , the NP adheres to the membrane shallowly through its cylindrical side [21]. As ξ is increased, they predicted a discontinuous transition to a deep wrapping state, in which the principal axis of the NP is perpendicular to the membrane regardless of the value of α or c_{edge} . This state is then followed, through another discontinuous transition, by full wrapping of the NP as ξ is further increased [21].

The goal of the present study is to investigate the modes of adhesion of spherocylindrical NPs and their endocytosis through an approach that accounts for thermal fluctuations. To this end, we used MD simulations of a coarse-grained implicit solvent model of self-assembled lipid membranes in which the lipid molecules as coarse-grained as short semi-flexible amphiphilic chains. To reduce the number of degrees of freedom associated with spherocylindrical NPs, they are modeled as a triangulated hollow shells. The focus of the study is to determine the phase diagram of adhesion and endocytosis of spherocylindrical NPs as a function of their aspect ratio, dimensions, and strength of the adhesive interaction.

II. MODEL AND NUMERICAL APPROACH

This work is based on a mesoscale implicit-solvent model for self-assembled lipid bilayers [27, 28], in which, a lipid molecule is coarse-grained into a short semi-flexible chain that is composed of one hydrophilic head (h) bead and two hydrophobic tail beads (t). The potential energy of the lipid bilayer has three contributions, and is given

by,

$$U(\{\mathbf{r}_{i}\}) = \sum_{i,j} U_{0}^{\alpha_{i}\alpha_{j}}(r_{ij}) + \sum_{\langle i,j\rangle} U_{\text{bond}}^{\alpha_{i}\alpha_{j}}(r_{ij}) + \sum_{\langle i,j,k\rangle} U_{\text{bend}}^{\alpha_{i}\alpha_{j}\alpha_{k}}(\mathbf{r}_{i},\mathbf{r}_{j},\mathbf{r}_{k}),$$
(1)

where \mathbf{r}_i is the coordinate of bead $i, r_{ij} = \mathbf{r}_i - \mathbf{r}_j$, and α_i (= h or t) represents the type of bead i. The second summation in Eq. (1) is over bonded pairs within the lipid chains, and the third summation is over the triplets of beads constituting each lipid chain. The first term in Eq. (1) is a soft two-body potential, between beads of types α and β . This interaction is given by Eq. (A2) in Appendix A of Ref. [29]. Due to the absence of explicit solvent in this model, the self-assembly of the lipid chains into bilayers is achieved through a short-range attractive interaction between the t beads. Otherwise, h-h and h-t interactions are repulsive [28].

In Eq. (1), $U_{\rm bond}^{\alpha\beta}$ is a harmonic potential which ensures that beads within a chain are connected, and is given by

$$U_{\text{bond}}^{\alpha\beta}(r) = \frac{k_{\text{bond}}^{\alpha\beta}}{2} (r - a_{\alpha\beta})^2, \qquad (2)$$

where $k_{\rm bond}^{\alpha\beta}$ is the bond stiffness coefficient. Finally, $U_{\rm bend}^{\alpha\beta\gamma}$ in Eqn. (1) is a three body potential that provides bending stiffness to the lipid chains, and is given by

$$U_{\text{bend}}^{\alpha\beta\gamma}(\mathbf{r}_i, \mathbf{r}_j, \mathbf{r}_k) = \frac{k_{\text{bend}}^{\alpha\beta\gamma}}{2} \left(\cos \varphi_0^{\alpha\beta\gamma} - \frac{\mathbf{r}_{ij} \cdot \mathbf{r}_{kj}}{r_{ij} r_{kj}} \right)^2, \quad (3)$$

where $k_{\rm bend}^{\alpha\beta\gamma}$ is the bending stiffness coefficient, and $\varphi_0^{\alpha\beta\gamma}$ is the preferred splay angle of the lipid chain taken to be 180°.

A spherocylindrical NP is constructed as a fairly rigid triangulated mesh following the details provided in Supplementary Material. The hemispherical caps are the two halves of a geodesic polyhedron, that is constructed starting from an icosahedron followed by three tessellations, followed then by the projection of the vertices onto a sphere [30]. The two hemispheres are then connected by a tessellated cylinder. Each vertex of the NP is occupied by a bead n. Every n bead of the NP is connected to its nearest neighbors by the harmonic potential, Eq. (2), with a bond stiffness k_{bond}^{nn} and a preferred bond length a_b^{nn} . The value of a_b^{nn} is determined from the initial configuration of the NP, as described in ESI. The rigidity of the NP is further enhanced through the three-body potential, given by Eq. (3), between the beads of every connected triplet, with a bending stiffness $k_{\rm bend}^{nnn}$. The preferred splay angle φ_0^{nnn} of each triplet is determined from the initial configuration of the NP. Since the NP is hollow, the two-body and three-body interactions are not sufficient to provide a very rigid structure to the NP.

This problem is solved by introducing an additional bead, c, at the center of mass of the NP, that is connected to each n bead by a harmonic bond given by Eq. (2), with a bond stiffness $k_{\rm bond}^{cn}$ and a bond length determined by the initial configuration. Short-range attractive interaction between the n beads of the NP and a lipid head bead is ensured using $U_{min}^{nh} < 0$. To prevent partial insertion of the NP in the hydrophobic core of the lipid bilayer, $U_{min}^{nt} = 0$.

The specific values of the model interaction parameters used in the simulations are given by,

$$\begin{array}{lll} U_{\rm max}^{hh} &= U_{\rm max}^{ht} = 100\epsilon, \\ U_{\rm max}^{tt} &= 200\epsilon, \\ U_{\rm min}^{hh} &= U_{\rm min}^{ht} = 0, \\ U_{\rm min}^{tt} &= -6\epsilon, \\ U_{\rm min}^{nh} &= U_{\rm max}^{nt} = 1210\epsilon, \\ U_{\rm min}^{nh} &= -\mathcal{E}, \\ U_{\rm min}^{nt} &= 0, \\ k_{\rm bond}^{ht} &= k_{\rm bond}^{tt} = 100\epsilon/r_m^2, \\ k_{\rm bend}^{ht} &= 100\epsilon, \\ \varphi_0^{htt} &= 180^{\circ}, \\ k_{\rm bond}^{nn} &= 500\epsilon/r_m^2, \\ k_{\rm bend}^{nn} &= 100\epsilon, \\ \varphi_0^{nnn} &= variable, \\ k_{\rm bond}^{cn} &= 10\epsilon/r_m^2, \\ k_{\rm bond}^{cn} &= 10\epsilon/r_m^2, \\ k_{\rm bond}^{cn} &= 10\epsilon/r_m^2, \\ k_{\rm bond}^{cn} &= variable. \end{array}$$

All beads are moved using a MD scheme in conjunction with a Langevin thermostat [31],

$$\dot{\mathbf{r}}_i(t) = \mathbf{v}_i(t), \tag{5}$$

$$m\dot{\mathbf{v}}_i(t) = -\nabla_i U - \Gamma \mathbf{v}_i(t) + \sigma \Xi_i(t), \tag{6}$$

where m is the mass of a bead and Γ is a bead's friction coefficient. $\sigma \Xi_i(t)$ is a random force with zero mean, and is uncorrelated for different particles, different times, and different components. Γ and σ are inter-related through the fluctuation-dissipation theorem leading to $\Gamma = \sigma^2/2k_{\rm B}T$. The simulations are performed in the $NVT\Sigma$ ensemble, where N is the total number of beads in the system, $V = L_x L_y L_z$ is the system's volume, and Σ is the lateral tension applied on the bilayer along the xy-plane with the constraint $L_x = L_y = L$. The projected size of the bilayer is adjusted through a Monte Carlo scheme in which an attempted new linear system size along the xy-plane, $L' = L + \Lambda$, is selected, with Λ being a small random perturbation in the interval $(-0.1r_m, 0.1r_m)$. Attempted new coordinates of all beads correspond then to $x_i' = x_i L'/L$, $y_i' = y_i L'/L$, and $z_i' = z_i L'/L$. The attempted change is then accepted or rejected using

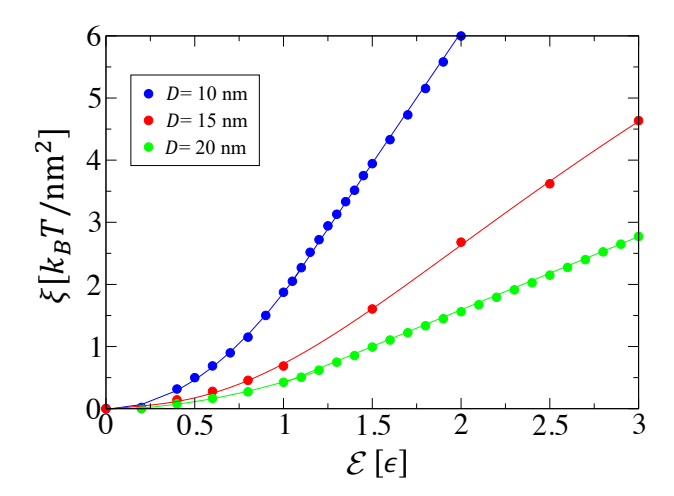


FIG. 1: The adhesion energy density, ξ , versus the interaction strength, \mathcal{E} , between a NP n bead and a lipid h bead, for different values of the NP's diameter.

the standard Metropolis criterion with the Hamiltonian $H(\{\mathbf{r}_i\}, L) = U(\{\mathbf{r}_i\}) + \Sigma L^2$. All simulations are performed on tensionless membranes $(\Sigma = 0)$. Typically the initial size $(L_x, L_y, L_z) = (100r_m, 100r_m, 100r_m)$. The total number of lipids in the membrane is $N_{lip} = 10000$.

The simulations are executed at $k_BT=3.0\epsilon$, with a time step $\Delta t=0.02\tau$, where $\tau=r_m(m/\epsilon)^{1/2}$. Eqs. (5 and 6) are integrated using the velocity-Verlet algorithm [32] with $\Gamma=\sqrt{6}m/\tau$. The bending modulus of the bare bilayer, with the interaction parameters given by Eq. (4), as extracted from the spectrum of the height fluctuations of the bilayer, is $\kappa\approx 30k_BT$ [28], which is comparable to that of a DPPC bilayer in the fluid phase [33]. By comparing the thickness of our model bilayer in the fluid phase, which is about $4r_m$, with that of a typical fluid phospholipid bilayer, ~ 4 nm, we estimate $r_m\approx 1$ nm. Hence, in the remainder of this article, all lengths are expressed in nanometers, and the adhesion strength, ξ , is expressed in k_BT/nm^2 .

The adhesion energy density is defined as ξ = $|U_{adh}|/A_{adh}$, where U_{adh} is the net potential energy between the NP and the membrane and A_{adh} is the area of the NP adhering to the membrane. To determine the adhesion energy density, simulations of a spherical NP of diameter D adhering to a tensionless planar bilayer are performed at different values of \mathcal{E} . Here, an n bead adheres to the membrane if it interacts with at least one h bead of the membrane, i.e. if its distance from the hbead is less than r_c . Fig. 1 depicts the adhesion energy density versus distance \mathcal{E} for NPs with diameter D=10, 15 and 20 nm. This figure shows that ξ dependence on \mathcal{E} is not linear for low values of \mathcal{E} , but becomes linear as \mathcal{E} further increases. This figure also shows that for a given \mathcal{E} , ξ decreases with D. This is simply due to the fact that the number of beads on a spherical NP is fixed (642 beads), regardless of its size.

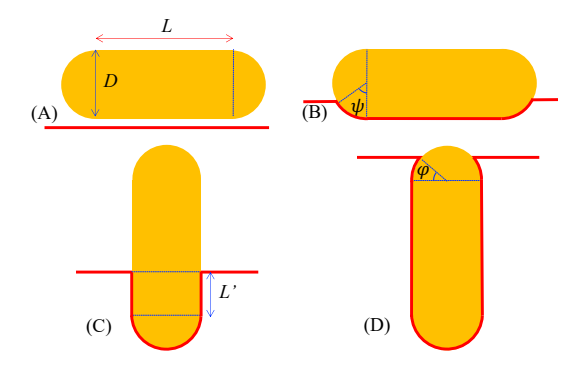


FIG. 2: The four adhesion modes of a spherocylindrical NP used in the theoretical determination of the phase diagram. (A) corresponds to the unbound state. (B) corresponds to the parallel adhesion mode. (C) corresponds to the perpendicular adhesion mode in which the NP's cylindrical side is partially wrapped by the membrane. Finally, (D) corresponds to the perpendicular adhesion mode in which the cylindrical side is fully wrapped and the top hemispherical cap is partially wrapped.

III. ELASTICITY THEORY PHASE DIAGRAM

Before presenting our results from the MD simulations, it is instructional to first determine an approximate adhesion phase diagram of a spherocylindrical NP using simplified theoretical arguments based on a balance between the Helfrich's curvature energy [34] of the membrane and the adhesion energy. Assuming that the NP only deforms the portion of the membrane that is in contact with it, the excess free energy of the membrane is then given by [34]

$$\mathcal{F} = \int_{-A}^{A} da \, \frac{\kappa}{2} (c_1 + c_2 - c_0)^2 + \int_{-A}^{A} da \, \tilde{\kappa} c_1 c_2 - \xi A, \quad (7)$$

where A is the NP-membrane contact area. κ and $\tilde{\kappa}$ are the bending modulus and saddle splay modulus, respectively. c_1 and c_2 are the local principal curvatures of the membrane in the contact region. Due to the absence of transbilayer asymmetry of the membrane, the spontaneous curvature $c_0 = 0$. Assuming that the saddle-splay bending modulus is not locally modified by the adhesion of the NP, the second term in Eq. (7) reduces to an integral of the Gaussian curvature c_1c_2 over space, which is a topological invariant. Therefore, this term is not included in the subsequent calculations.

Motivated by the MD results, four adhesion modes of the NP on the membrane, shown schematically in Fig. 2 are considered in the calculations. These correspond to the unbound state, the parallel adhesion mode, the partially wrapped perpendicular mode, and the strongly wrapped perpendicular mode, shown by (A), (B), (C), and (D), respectively. The free energy of the system in

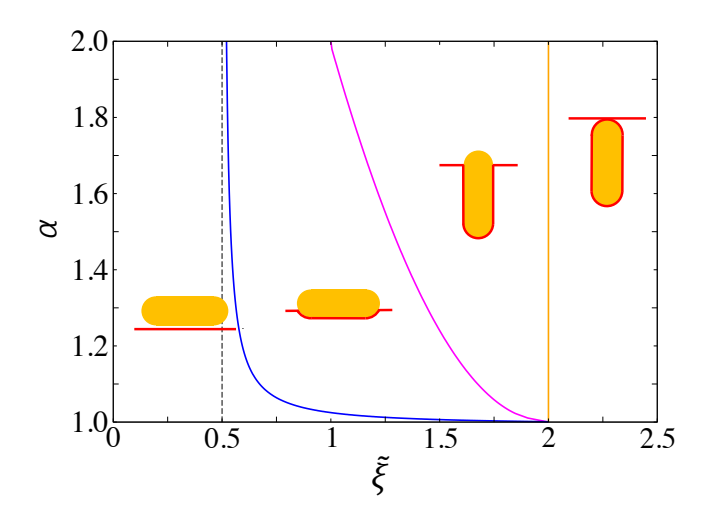


FIG. 3: Theoretical adhesion phase diagram in terms of the reduced adhesion energy density, $\tilde{\xi}$, and NP's aspect ratio, α , obtained from the minimization of the free energy given by Eq. (8). The transition line from the unbound mode to the parallel mode is blue, the transition line from the parallel mode to the perpendicular mode is pink, and the transition line from the perpendicular mode to the fully wrapped mode is orange. Note that the transition line from the unbound to the parallel mode (blue line) asymptotically approaches the adhesion threshold of a an infinitely long cylindrical NP ($\tilde{\xi}=0.5$) as α is increased.

the different modes is given by

$$\frac{\mathcal{F}}{2\pi\kappa} = \begin{cases} 0 & \text{for (A),} \\ (2 - \tilde{\xi})(1 - \cos\psi) + \frac{\alpha - 1}{\pi}(1 - 2\tilde{\xi})\psi & \text{for (B),} \\ (2 - \tilde{\xi}) + (\alpha' - 1)(1 - 2\tilde{\xi}) & \text{for (C),} \\ (2 - \tilde{\xi})(1 + \sin\varphi) + (\alpha - 1)(1 - 2\tilde{\xi}) & \text{for (D),} \end{cases}$$
(8

where $\tilde{\xi} = \xi D^2/4\kappa$ is the reduced adhesion energy density, D is the NP's diameter, $\alpha = (L+D)/D$ is the NP's aspect ratio, and $\alpha' = (L'+D)/D$, where L' is the partial height of the cylindrical portion of the NP that is wrapped by the membrane. The wrapping angles ψ and φ are defined in Fig. 2. We emphasize that this theoretical approach is fairly crude as (1) it assumes that the interaction between the NP and the membrane is a contact interaction, (2) it does not account for the fact that the NP deforms the membrane beyond the contact region, (3) it is only valid in the limit where the NP's dimensions are much larger than the membrane thickness, and (4) it does not account for fluctuations.

The phase diagram of the adhesion modes, in terms of $\tilde{\xi}$ and α , obtained from the minimization of the free energy in Eq. (8) is shown in Fig. 3. The degree of wrapping of the NP f, defined as the fraction of the NP's area that is wrapped by the membrane, is shown as a function of $\tilde{\xi}$ for four different values of the aspect ratio in Fig. 4.

Fig. 3 shows that regardless of the aspect ratio, the NP adheres to the membrane in the parallel mode at low

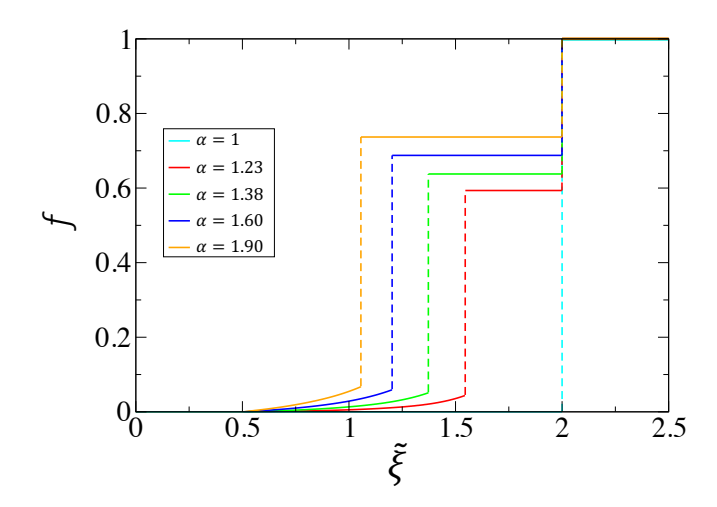


FIG. 4: The degree of wrapping of the NP's area, obtained from the minimization of the free energy in Eq. (8), as a function of the reduced adhesion energy density, for different values of the aspect ratio.

values of the adhesion energy density. In this state, the degree of wrapping f gradually increases with increasing ξ toward a maximum value that increases with the aspect ratio, as shown by Fig. 4. This is contrasted to the case of a spherical NP ($\alpha = 1$ in Fig. 3), which can either be unbound (f = 0) or completely wrapped (f = 1). The cylindrical side of a spherocylindrical NP therefore allows for its partial wrapping. As the adhesion strength is further increased, the NP mode of adhesion changes to the perpendicular mode, in which the whole cylindrical side of the NP is wrapped by the membrane (i.e. L' =L). The phase diagram also shows that the adhesion energy density, at which the NP flips from the parallel to the perpendicular mode, decreases with increasing the aspect ratio. Interestingly, the range of ξ over which the parallel mode is stable decreases with increasing α , and eventually vanishes in the marginal case of infinitely long NPs. The transition from the perpendicular mode to the fully wrapped mode occurs at $\tilde{\xi} = 2$ regardless of the NP's aspect ratio, and includes the case of a spherical NP. In state (D), the NP is always fully wrapped, i.e. $\varphi = \pi/2$ regardless of $\tilde{\xi}$.

IV. NUMERICAL RESULTS

We now turn to the modes of adhesion, obtained from the MD simulations. Fig. 5 depicts a sequence of typical equilibrium configurations for different values of the adhesion energy density in the case of $\alpha=1.60$. These modes of adhesion are essentially the same as those in Fig. 2, with some differences which will be discussed later. The endocytosis mode in Fig. 5 at $\xi=1.56k_BT/\text{nm}^2$ is identified with the completely wrapped state in Fig. 2.

The adhesion phase diagram, from the simulations, as

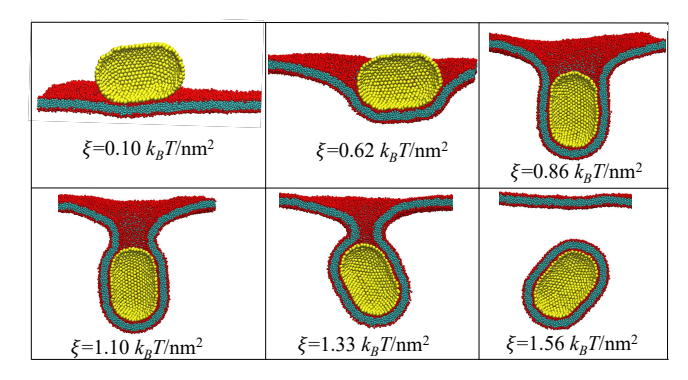


FIG. 5: Equilibrium snapshots at different values of ξ in the case of a NP with D=20 nm and $\alpha=1.60$.

a function of the adhesion energy density and aspect ratio in the case of NPs with D=20 nm is shown in Fig. 6. The degree of wrapping of the NP as a function of adhesion energy density for different values of aspect ratio for D=20 nm is shown in Fig. 7. Fig. 6 shows a ξ - α phase diagram of adhesion that is qualitatively in agreement with the theoretical one in Fig. 3. Namely, the NP is unbound at very low values of ξ and adheres in the parallel mode as ξ is increased. As ξ is further increased, the NP adheres in the perpendicular mode, and is endocytosed at high values of ξ . The qualitative dependence of the transition lines on ξ from the MD simulations agree with those in Fig. 3. In particular, the transition adhesion energy density from the unbound state to the parallel adhesion mode and that from the parallel to the perpendicular mode decrease with increasing the aspect ratio.

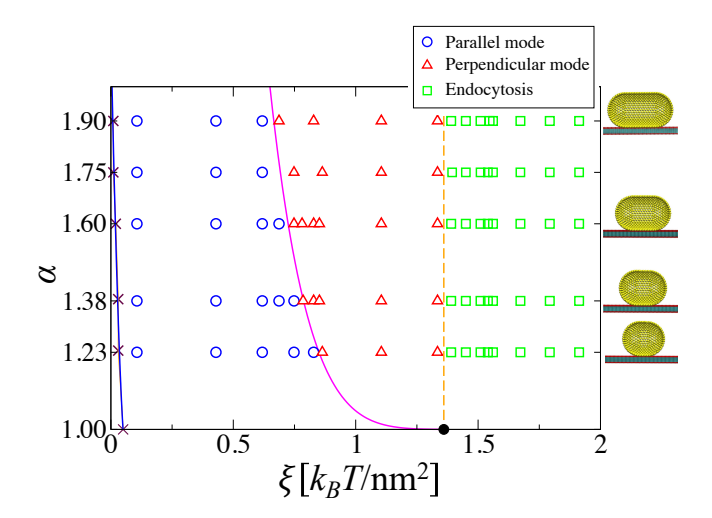


FIG. 6: ξ - α adhesion phase diagram, from the MD simulations, in the case of D=20 nm. The transition line from the unbound state to the parallel adhesion mode is blue, the transition line from the parallel mode to the perpendicular mode is pink and the transition line from the perpendicular mode to endocytosis is orange.

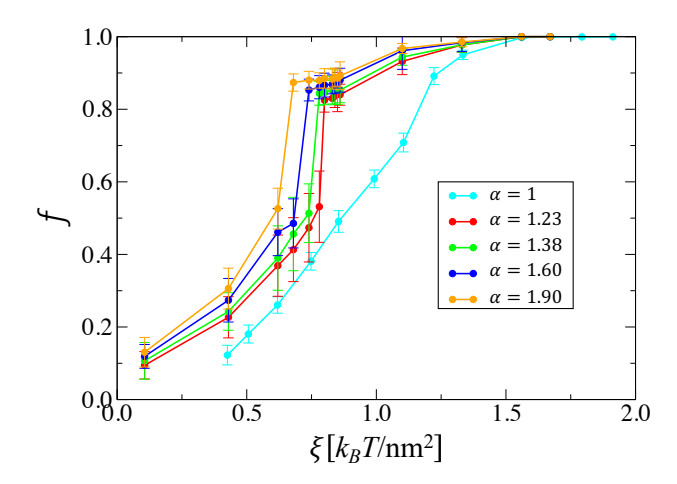


FIG. 7: The degree of wrapping of the NP versus ξ for the case of D=20 nm at different values of the NP's aspect ratio. Here, a NP bead is in contact with the membrane if it is at a distance ≤ 2 nm with at least one membrane head bead.

These results imply that the higher is the aspect ratio of a spherocylindrical NP, the easier it is for it to adhere to a planar membrane. Likewise, the NP becomes more prone to flip from the parallel to the perpendicular mode as its aspect ratio is increased. Fig. 7 shows that the degree of wrapping exhibits a discontinuity at the transition from the parallel mode to the perpendicular mode, also in qualitative agreement with the theoretical predictions.

A notable qualitative difference between the MD and theoretical phase diagrams is that a spherical NP ($\alpha =$ 1), in the MD simulations, is partially wrapped over a range of values of ξ , with the contact area fraction f that increases continuously with ξ , as shown by the cyan data in Fig. 7 and by earlier studies [25, 26]. In contrast, the theoretical argument predicts that the NP is either unbound or completely wrapped, as demonstrated by the phase diagram in Figs. 3 and 4 at $\alpha = 1$. Another important difference between the phase diagrams in Figs. 3 and 6, is that the theoretical arguments predict that the degree of wrapping of the NP in the perpendicular mode is independent of ξ , as shown by Fig. 4. This is due to the fact that the theory predicts that the top hemispherical cap of the NP is not wrapped by the membrane in this mode. In contrast, the MD simulations show that the degree of wrapping increases continuously in the perpendicular mode, as shown by Fig. 6.

The effect of the NP's diameter on its adhesion is shown by the ξ -1/ D^2 phase diagram in Fig. 8 for the case of $\alpha=1.75$. The corresponding phase diagram is found in Supplementary Material. This figure shows that the adhesion energy densities corresponding to the transition from the parallel to the perpendicular mode and the transition from the perpendicular mode to endocytosis decrease with the diameter of the NP. Fig. 8 shows that the adhesion energy density at these transitions, $\xi^* \sim 1/D^2$, in agreement with the theoretical

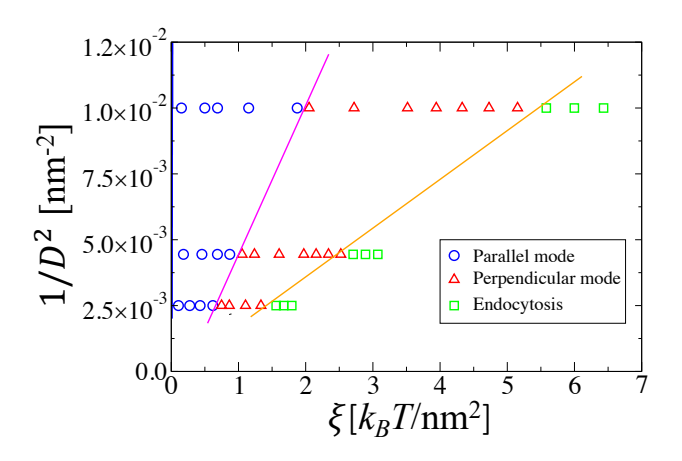


FIG. 8: ξ -1/ D^2 adhesion phase diagram, from the MD simulations, in the case of $\alpha=1.75$. The transition line from the unbound state to the parallel adhesion mode is blue, the transition line from the parallel mode to the perpendicular mode is pink, and the transition line from the perpendicular mode to endocytosis is orange. Note that the blue line is very close to the vertical axis.

predictions. The particularly strong dependence of ξ^* on the NP's diameter at the transition from the perpendicular mode to endocytosis, and the lack of dependence of ξ^* on the length of the NP, as shown by the ξ - α phase diagram in Fig. 6, imply that the onset of endocytosis of spherocylindrical NPs is controlled by their diameter and not by their length.

In the parallel mode, the NP's orientation is mainly parallel to the xy-plane, as shown by the distribution of the latitude angle, $P(\theta)$, depicted in Fig. 9 (A) for the case of D=20 nm and $\alpha=1.60$. We note that the normalization of P is $\int_0^\pi P(\theta) \sin\theta \ d\theta = 1/2\pi$. This figure shows that the distribution is peaked at $\theta=90^\circ$, which is consistent with a NP adhesion in the parallel mode. However, the amount of fluctuations exhibited by the NP's orientation increases with increasing the adhesion strength. This implies that as the transition from the parallel mode to the perpendicular mode is approached, the NP's wobbling around its horizontal orientation is increased.

The simulations show that in the perpendicular mode, the NP typically adopts an orientation in which its principal axis is almost parallel to the z-axis for relatively low values of ξ (see snapshot at $\xi=0.86k_BT/\mathrm{nm}^2$ in Fig. 5). However, for relatively high values of ξ , the NP's principal axis is mostly tilted with respect to the z-axis, as shown by the snapshot at $\xi=1.33k_BT/\mathrm{nm}^2$ in Fig. 5 and by the distribution of θ in Fig. 9 (B). To infer the origin of the tilt of the NP in the the perpendicular mode, the net adhesion potential energy of the NP vs. its latitude angle is shown in the scatter plot in Fig. 10, determined from a large set of configurations at equilibrium. This figure shows that for low values of ξ , within the perpendicular state, the range of the NP's latitude angle is small, for

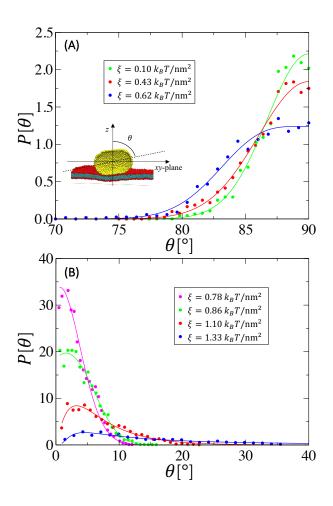


FIG. 9: (A) Distribution of the latitude angle θ , defined in the inset, for an NP with D=20 nm and $\alpha=1.60$ in the (A) parallel mode and (B) perpendicular mode, at different values of the adhesion energy density. The solid lines are guides to the eye.

example up to about 15° and an average about 5° for $\xi = 0.86k_BT/\mathrm{nm}^2$. This indicates that the NP's principal axis is mostly perpendicular to the xy-plane at low values of ξ within the perpendicular mode. However, as ξ is increased, the range of the latitude angle sampled by the NP is increased, with an average value about 18° at $\xi = 1.10k_BT/\mathrm{nm}^2$ and 23° at $\xi = 1.33k_BT/\mathrm{nm}^2$, which indicates a preferred tilt of the NP in the perpendicular mode at high ξ .

The adhesion energy, shown in Fig. 10, is essentially independent of the angle θ for a given ξ . This is explained by the fact that as the latitude angle θ of the NP changes, the size of the neck connecting the bud containing the NP to the membrane remains roughly constant, and therefore the amount of NP's wrapping is independent of θ . Since the curvature of the membrane in the contact region also remains unchanged by the tilt of the NP, the preferred tilt must be due to a reduced curvature energy of the non-contact region of the membrane. An interesting feature of the tilted orientation of the NP (see snapshots in

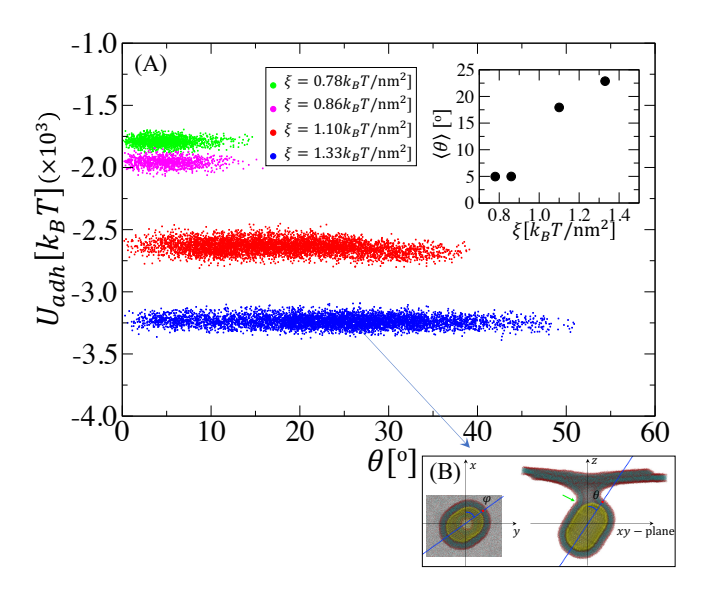


FIG. 10: Scatter plot of the NP's net adhesion energy, U_{adh} , versus its tilt angle θ for the case of D=20 nm, $\alpha=1.6$ at $\xi=1.33k_BT/\mathrm{nm}^2$. The inset shows that the average latitude angle of the NP versus adhesion energy density.

Fig. 10) is that at the azimuthal angle corresponding to the tilt angle θ , the membrane does not adhere to the top hemispherical cap, whereas at the supplementary azimuthal angle, the membrane degree of wrapping of the top hemispherical cap is maximized. Such a configuration must correspond to a reduced curvature energy of the non-contact region of the membrane than in the case where the NP is perpendicular to the xy-plane.

V. KINETICS OF ENDOCYTOSIS OF SPHEROCYLINDRICAL NPS

In this section, we focus on the effect of the adhesion energy density, aspect ratio and diameter of the NP on the kinetics of its endocytosis. Fig. 11 depicts the time evolution of the NP's latitude angle along with the fraction of its area wrapped by the membrane for the case of D=20 nm and $\alpha=1.6 \text{ at different values of } \xi \text{ within}$ the endocytosis regime. Here, the NP is initially placed such as its axis is perpendicular to the membrane (i.e. $\theta(0) = 0$). Time series of snapshots corresponding to $\xi = 1.56$ and $2.77k_BT/\text{nm}^2$ are also shown in Fig. 11. A corresponding movie is found in Supplementary Material. This figure shows that regardless of the adhesion strength, upon its adhesion on the membrane via one of its hemispherical caps, the NP rotates from the perpendicular to the parallel orientation within a short amount time. While the NP remains temporarily in the parallel orientation for a short duration, the degree of wrapping f, at which the orientation of the NP is parallel to the xy-plane increases with time, with a value around 0.5. The NP's latitude angle then decreases with time, as the

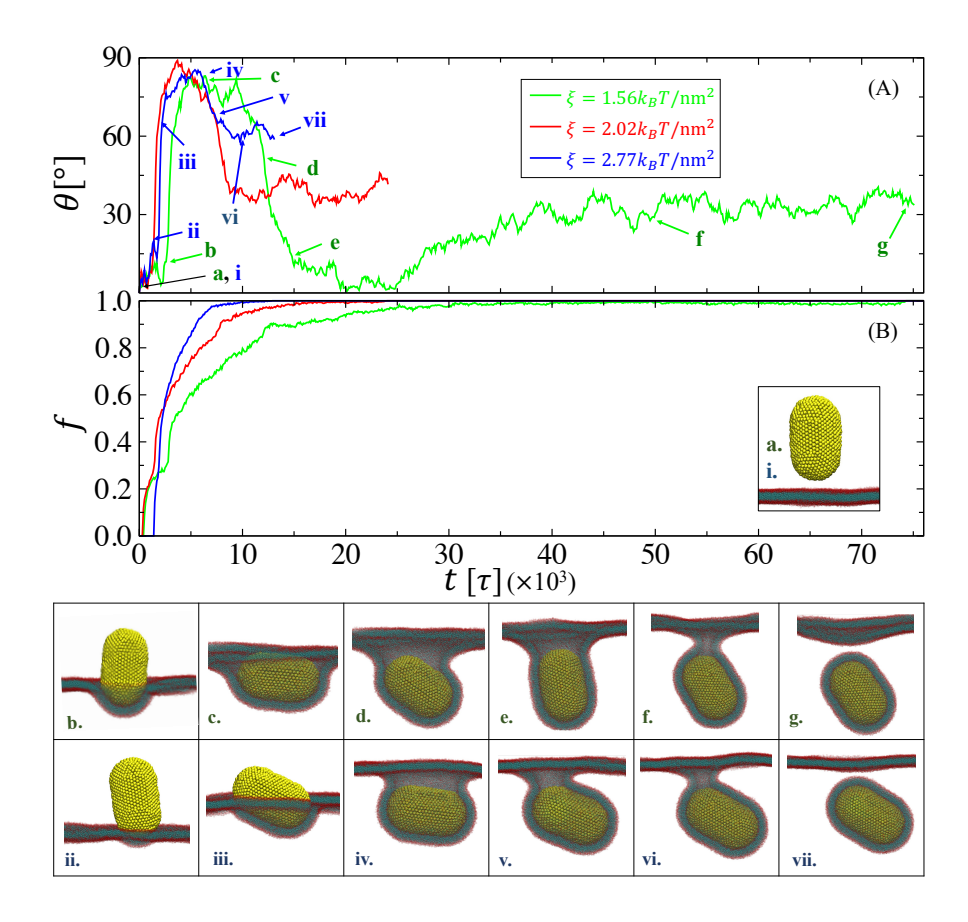


FIG. 11: (A) Latitude angle of the NP's principal axis versus time for the case of $\alpha=1.75$ and D=20 nm at three different values of the adhesion energy density. (B) The area fraction of the NP wrapped by the membrane versus time for the same systems shown in (A). Snapshot series (a) to (g) correspond to the case of $\xi=1.56k_BT/\mathrm{nm}^2$. Corresponding Multimedia view: link. Snapshot series (i) to (vii) correspond to the case of $\xi=2.77k_BT/\mathrm{nm}^2$. Corresponding Multimedia view: link. Snapshots (g) and (vii) are taken right after endocytosis.

degree of wrapping further increases. For relatively low values of ξ , such as $\xi=1.56k_BT/\mathrm{nm}^2$ (i.e. values of ξ close to the endocytosis transition line in the phase diagram), the NP almost completely rotates again to an orientation perpendicular to the xy-plane (snapshot (e) in Fig. 11). However, as the amount of wrapping increases, such as the neck connecting the main bilayer to the invagination containing the NP is well formed, the latitude angle increases again such as the NP adopts a tilted orientation (snapshot (f) in Fig. 11) that is reminiscent of that in the perpendicular adhesion mode at high values of ξ (snapshot at $\xi=1.33k_BT/\mathrm{nm}^2$ in Fig. 5). This kinetic pathways is in agreement with that observed by Huang $et\ al.\ [20]$ using a more coarse-grained model.

At higher values of ξ (e.g. $\xi = 2.02$ and $2.92k_BT/\text{nm}^2$), Fig. 11 and corresponding movie in Supplementary Material show that the NP does not rotate almost completely to the perpendicular orientation (snapshots (iv to vi) in Fig. 11), with the minimum value of θ achieved by the NP that increases with increasing ξ . This is due to the fact that the higher curvature energy of the intermediate orientations (iv-to vi) is compensated by a higher adhe-

sion energy (in absolute value) at high values of ξ . As a result, the NP is endocytosed while nearly parallel to the membrane at high values of ξ . The details of the endocytosis pathway therefore depends on the adhesion strength.

The effect of the diameter of the NP on the endocytosis kinetics is shown in Fig. 12 for the case of $\alpha = 1.75$ at $\xi = 6k_BT/\text{nm}^2$. Here, the NPs are initially placed parallel to the membrane. This value of ξ is very close to the endocytosis transition for D = 10 nm, as shown by the phase diagram in Fig. 8. Fig. 12 shows that the tendency of the NP to rotate from the horizontal orientation decreases with the difference, $\Delta \xi = \xi - \xi_{end}(D)$, where $\xi_{end}(D)$ is the value of the adhesion energy density at the endocytosis transition for a NP of diameter D. This is due to the fact that as D is increased, $\Delta \xi$ is increased, and therefore the resistance to wrapping of the NP by the membrane, due to the curvature energy is decreased. As a result the angle by which the NP rotates toward the perpendicular orientation is diminished as Dis increased.

VI. SUMMARY AND CONCLUSION

The adhesion modes and endocytosis of spherocylindrical NPs on tensionless planar membranes are investigated using molecular dynamics simulations of a coarsegrained implicit-solvent model. The NPs are efficiently modeled as triangulated hollow shells. The simulations were performed over a range of values of the NP's diameter D, aspect ratio α , and strength of the adhesion energy density ξ . The NPs exhibits two modes of adhesion which depend on ξ , α and D. For low values of ξ , the NP adheres through its side, i.e. its principal axis is parallel to the membrane with an increasing amount of wobbling with increasing ξ . As ξ is increased, the NP's adhesion mode flips to the perpendicular mode, in which the principal axis is mainly perpendicular to the membrane. The value of ξ corresponding to the transition from the parallel mode to the perpendicular mode decreases with increasing the NP's aspect ratio or its diameter, in agreement with theoretical arguments based on the Helfrich Hamiltonian. An interesting feature of the perpendicular adhesion mode is that once the neck of the bud containing the NP is well formed, the NP's principal axis is tilted from the z-axis by an angle that increases with ξ . The lack of correlation between this tilt angle and the net adhesion energy of the NP implies that the preferred tilt angle in the perpendicular adhesion mode is due to a combination of the finite range of the interaction between the lipid head beads and the NP and the curvature energy of the non-contact region of the membrane.

The sequence of adhesion modes observed in this study are in qualitative agreement with those based on the energy minimization approach [21]. However, in their approach, the NPs caps are blunt with varying degrees. Due to the bluntness of the caps, the transition between the partially wrapped perpendicular mode and the fully

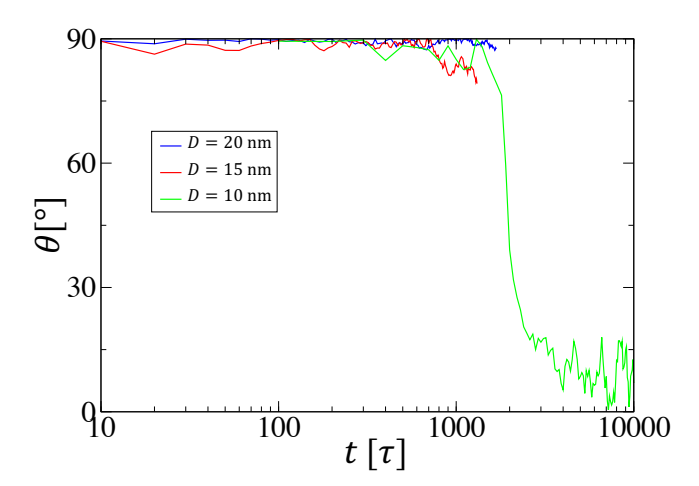


FIG. 12: Latitude angle of the NP's principal axis versus time for the case of $\alpha = 1.75$ and $\xi = 6k_BT/\text{nm}^2$ at three values of the NP's diameter.

wrapped perpendicular mode is discontinuous. In contrast, the present study shows that the degree of wrapping increases continuously with increasing ξ .

As ξ is further increased, the NP undergoes spontaneous endocytosis. The value of ξ corresponding to the transition from the perpendicular adhesion mode to endocytosis (ξ_{end}) is found to be independent from the NP's aspect ratio. However, ξ_{end} decreases with the diameter, as $1/D^2$, in agreement with the theoretical arguments. The independence of the this transition from the NP's aspect ratio is due to the fact that the neck linking the NP's invagination to the main membrane in the perpendicular mode is near the hemispherical cap, and is therefore independent of the length of the cylindrical portion.

The kinetics of endocytosis depends strongly on ξ and D. Quickly after its adhesion, the NP rotates to a parallel orientation until its degree of wrapping is about 0.5. The NP then rotates toward the perpendicular orientation while its degree of wrapping increases with time. A minimum orientation angle of almost 0 is achieved in the case of relatively weak values of ξ . The almost vertical orientation of the NP is achieved once the cylindrical portion of the NP is fully wrapped. As the degree of wrapping further increases, the tilt of the NP's orientation increases. This implies that as the NP's invagination detaches from the membrane, the NP is not perpendicular to the xy-plane at low values of ξ . As ξ is increase, within the endocytosis region of the phase diagram, the minimum angle it achieves, as it rotates away from its parallel orientation, decreases with increasing ξ . As such, the NP's orientation as it is endocytosed becomes increasingly parallel to the xy-plane as \mathcal{E} is increased. The tendency of the NP to rotate from the parallel mode to the perpendicular mode during its endocytosis pathway is also found to decrease with increasing its diameter. However, it is fairly independent of its aspect ratio. The observed endocytosis pathways agree with earlier ones performed in the limit of high adhesion strength [19] and in the limit of relatively weak adhesion strength [20].

Supplementary Material

See Supplementary Material for 1) a detailed description on how spherocylindrical nanoparticles are generated in this study, 2) a ξ -D phase diagram, 3) a movie of the endocytosis of a nanoparticle with $\alpha=1.75$, D=20 nm at $\xi=1.56k_BT/\mathrm{nm}^2$, and 4) a movie of the endocytosis of a nanoparticle with $\alpha=1.75$, D=20 nm at $\xi=2.77k_BT/\mathrm{nm}^2$.

Acknowledgements

This work was supported by a grant from the National Science Foundation (DMR-1931837). All simulations were performed on computers of the High Performance Computing Facility at the University of Memphis.

Snapshots in this article were generated using VMD version 1.9.3 [35].

request.

Data Availability

The data that support the findings of this study are available from the corresponding author upon reasonable

- N. Baig, I. Kammakakam, and W. Falath, Mater. Adv. 2, 1821 (2021).
- [2] M. Falahati, F. Attar, M. Sharifi, A.A. Saboury, A. Salihi, F. M. Aziz, I. Kostova, P. Priecel, J.A. Lopez-Sanchez, S. Laurent, N. Hooshmand, and M.A. El-Sayed, Biochim. Biophys. Acta 1864, 129435 (2020).
- [3] X. Wu, C. Hao, J. Kumar, H. Kuang, N.A. Kotov, L.M. Liz-Marzán, and C. Xu, Chem. Soc. Rev. 47, 4677 (2018).
- [4] W. Wu, Nanoscale 9, 7342 (2017).
- [5] M. Gu, Q. Zhang, and S. Lamon, Nat. Rev. Mater. 1, 16070 (2016).
- [6] D.J. McClements and H. Xiao, npj Sci. Foods 1, 6 (2017).
- [7] L. Salvioni, L. Morelli, E. Ochoa, M. Labra, L. Fiandra, L. Palugan, D. Prosperi, and M. Colombo, Adv. Coll. Int. Sci. 293, 1023437 (2021).
- [8] K. Wang, F. M. Kievit, and M. Zhang, Pharmacol. Res. 114, 56 (2016).
- [9] T. Sun, Y. S. Zhang, B. Pang, D. C. Hyun, M. Yang, and Y. Xia, Ang. Chem. 53, 12320 (2014).
- [10] A. J. Mieszawska, W. J. M. Mulder, Z. A. Fayad, and D. P. Cormode, Mol. Pharmaceutics 10, 831 (2013).
- [11] J. N. Anker, W. P. Hall, O. Lyandres, N. C. Shah, J. Zhao, and R. P. Van Duyne, Nat. Mat. 7, 442 (2008).
- [12] L.A. Austin, B. Kang, and M.A. El-Sayed, Nano Today. 10, 542 (2015).
- [13] P.R. Leroueil, S. Hong, A. Mecke, J.R. Baker Jr., B.G. Orr, and M.M. Banaszak Holl, Acc. Chem. Res. 40, 335 (2007).
- [14] B.J. Marquis, S.A. Love, K.L. Braun, C.L. Haynes, Analyst 134, 425 (2009).
- [15] X. Lu, Y. Liu, X. Kong, P.E. Lobie, C. Chen, T. Zhu, Small 9, 1654 (2013).
- [16] J.E. Ortiz-Castillo, R.C. Galo-Villanueva, M.J. Madou, and V.H. Perez-Gonzalez, Coord. Chem. Rev. 425, 213489 (2020).
- [17] B.D. Chithrani, A.A. Ghazani, and W.C. Chan, Nano

- Lett. **6**, 662 (2006).
- [18] S.E.A. Gratton, P.A. Ropp, P.D. Pohlhaus, J.C. Luft, V.J. Madden, M.E. Napier, and J.M. DeSimone, Proc. Natl. Acad. Sci. U.S.A. 105, 11613 (2008).
- [19] R. Vácha, F. J. Martinez-Veracoechea, and D. Frenkel, Nano Lett. 11, 5391 (2011).
- [20] C. Huang, Y. Zhang, H. Yuan, H. Gao, and S. Zhang, Nano Lett. 13, 4546 (2013).
- [21] S. Dasgupta, T. Auth, and G. Gompper, Nano Lett. 14, 687 (2014).
- [22] R. Lipowsky and H.-G. Döbereiner, Europhys. Lett. 43, 219 (1998).
- [23] M. Deserno, and T. Bickel, Europhys. Lett. 62, 767 (2003).
- [24] M. Raatz, R. Lipowsky, and T.R. Wiekl, Soft Matter 10, 3570 (2014).
- [25] E.J. Spangler, S. Upreti, and M. Laradji, J. Chem. Phys. 144, 044901 (2016).
- [26] E.J. Spangler and M. Laradji, J. Chem. Phys. 152, 104902 (2020).
- [27] J. D. Revalee, M. Laradji and P. B. Sunil Kumar, J. Chem. Phys. 28, 035102 (2008).
- [28] M. Laradji, P. B. Sunil Kumar and E. J. Spangler, J. Phys. D.: Appl. Phys. 49, 293001 (2016).
- [29] E. J. Spangler and M. Laradji, J. Chem. Phys. 154, 244902 (2021).
- [30] J.R. Baumgardner, and P.O. Frederickson, SIAM J. Numer. Anal. 22, 1107 (1985).
- [31] G.S. Grest and K. Kremer, Phys. Rev. A 33, 3628 (1986).
- [32] W.C. Swope, H.C. Andersen, P.H. Berens. and K.R. Wilson, J. Chem. Phys. 76, 637 (1982).
- [33] J.F. Nagle, M.S. Jablin, S. Tristram-Nagle, and K. Akabori, Chem. Phys. Lipids 185, 3 (2015).
- [34] W. Helfrich, Z. Naturforsch. 28c, 693 (1973).
- [35] W. Humphrey, A. Dalke, and K. Schulten, J. Mol. Graphics 14, 33 (1996).